RSC Medicinal Chemistry

ROYAL SOCIETY OF CHEMISTRY

RESEARCH ARTICLE

View Article Online
View Journal | View Issue

Cite this: *RSC Med. Chem.*, 2023, **14**, 2315

Novel styryl-thiazole hybrids as potential anti-Alzheimer's agents†

Niki Gouleni,[a] Annalisa Di Rienzo,[b] Ahmet Yılmaz,[c] Harun Selvitopi,[d] Mehmet Enes Arslan,[c] Adil Mardinoglu,[ef] Hasan Turkez,[g] Antonio Di Stefano,[b] Stamatia Vassiliou*[a] and Ivana Cacciatore *[b]

In this study, combining the thiazole and cinnamoyl groups into the styryl-thiazole scaffold, a series of novel styryl-thiazole hybrids (**6a–p**) was rationally designed, synthesized, and evaluated by the multi-target-directed ligands strategy as potential candidates for the treatment of Alzheimer's disease (AD). Hybrids **6e** and **6i** are the most promising among the synthesized hybrids since they are able to significantly increase cell viabilities in $A\beta_{1-42}$-exposed-human neuroblastoma cell line (**6i** at the concentration of 50 μg mL^{-1} and **6e** at the concentration of 25 μg mL^{-1} resulted in ~34% and ~30% increase in cell viabilities, respectively). Compounds **6e** and **6i** exhibit highly AChE inhibitory properties in the experimental AD model at 375.6 ± 18.425 mU mL^{-1} and 397.6 ± 32.152 mU mL^{-1}, respectively. Moreover, these data were also confirmed by docking studies and *in vitro* enzyme inhibition assays. Compared to hybrid **6e** and according to the results, **6i** also has the highest potential against $A\beta_{1-42}$ aggregation with over 80% preventive activity. The *in silico* prediction of the physicochemical properties confirms that **6i** possesses a better profile compared to **6e**. Therefore, compound **6i** presents a promising multi-targeted active molecular profile for treating AD considering the multifactorial nature of AD, and it is reasonable to deepen its mechanisms of action in an *in vivo* experimental model of AD.

Received 4th July 2023,
Accepted 18th September 2023

DOI: 10.1039/d3md00308f

rsc.li/medchem

Introduction

In the last decades sulfur-containing therapeutics, such as glutathione, lipoic acid, and other thiol derivatives, have been widely investigated for the treatment of neurogenerative diseases such as Parkinson's (PD) or Alzheimer's diseases (AD).[1–3] Notably, sulfur pharmacophores were conjugated or merged with other molecules endowed with anti-inflammatory, antioxidant, anti-Aβ-aggregation, anti-acetylcholinesterase, and anti-MAO activities in order to act on multiple targets involved in the onset and/or progression of these pathologies.[4–6]

Heterocyclic rings are commonly used in the drug design of biologically active substances.[7–9] Recently thiazole-based derivatives were proposed as potential lead compounds for the development of novel cholinesterase inhibitors or receptors for advanced glycation end-products (RAGE) antagonists.[10–12] It was reported that the thiazole ring was able to create crucial interactions with the amino acid residues at the level of the active site of AChE.[13] However, if on one hand the potential role of the thiazole scaffold as a cholinesterase inhibitor was widely explored, on the other hand, literature data about its potential as a multitarget AD therapeutic are very scarce.

Based on the above-mentioned evidence and considering the multifactorial nature of AD, it is reasonable to design novel styryl-thiazole hybrids able to interact with multiple targets involved in the pathogenesis of AD.[14,15]

This paper reports the synthesis of novel styryl-thiazole hybrids obtained by the fusion of two pharmacophoric groups capable of interacting with the active site of AChE (thiazole ring) and counteracting the inflammatory and antioxidant status of the cerebral areas of the brain affected by AD (cinnamic acid). Cinnamic acid and its derivatives display a broad spectrum of biological activities and they

[a] *Laboratory of Organic Chemistry, Department of Chemistry, National and Kapodistrian University of Athens, Athens, Greece*
[b] *Department of Pharmacy, "G. D'Annunzio" University of Chieti-Pescara, 66100, Chieti Scalo, CH, Italy. E-mail: ivana.cacciatore@unich.it*
[c] *Department of Molecular Biology and Genetics, Faculty of Science, Erzurum Technical University, 25050, Erzurum, Turkey*
[d] *Department of Mathematics, Faculty of Sciences, Erzurum Technical University, 25050, Erzurum, Turkey*
[e] *Science for Life Laboratory, KTH-Royal Institute of Technology, SE-17121 Stockholm, Sweden*
[f] *Centre for Host-Microbiome Interactions, Faculty of Dentistry, Oral & Craniofacial Sciences, King's College London, London SE1 9RT, UK*
[g] *Department of Medical Biology, Faculty of Medicine, Atatürk University, Erzurum, Turkey*

† Electronic supplementary information (ESI) available: NMR spectra and HPLC chromatograms of **6a–p**. See DOI: https://doi.org/10.1039/d3md00308f

have been studied as anti-AD agents due to their anti-neuroinflammatory properties and their ability to inhibit Aβ aggregation by scavenging oxidants.[16,17] However, the use of cinnamic acid is restricted by its poor water solubility, low oral bioavailability, and scarce capability to cross the blood–brain barrier (BBB).[18]

The incorporation of sulfur pharmacophore into the hybrid can enhance the pharmacokinetic properties of cinnamic acid along with the engagement of several targets involved in the multifaceted pathophysiology of AD resulting in an effective approach toward AD therapy. The thiazole group was merged with the styryl portion of cinnamic acid using the hybridization strategy schematically reported in Fig. 1. Starting from the basic scaffold – represented by (*E*)-2-styryl thiazole – a structure–activity relationships study was performed introducing a series of small substituents with different chemical–physical properties (steric hindrance, electron-donating or -withdrawing effects, hydrophilicity) on both thiazole and benzene rings. The synthesized hybrids **6a–6p** were assessed by the neuroprotective effects on Aβ-neurotoxicity induced on SHSY-5Y neuroblastoma cells, AChEs inhibition, β-secretase inhibition, and genotoxic properties. ADME properties were also evaluated using Swiss ADME tool.

Results and discussion

Chemistry

The synthetic pathway toward the synthesis of *E*-styryl thiazoles **6a–p** is outlined in Scheme 1. Cinnamamides **2a–h** were efficiently prepared from cinnamic acids **1a–h** through a two-step procedure.[19–21] The acids were converted to their succinic esters using EDC·HCl and *N*-hydroxysuccinimide (NHS) in CH_2Cl_2 at room temperature. The crude active ester was subsequently converted to the corresponding amide after slow addition of 25% aq. NH_3 in a biphasic system formed by a solvent mixture $CHCl_3/CH_3CN$ (1 : 2). Thionation of the amides with Lawesson's reagent resulted ineffective. On the other hand, heating amides **2a–h** at 80 °C in dry dioxane in the presence of P_2S_5 (the reaction was followed by TLC) provided thioamides **3a–h** in medium yields (17–60%) after column chromatography.[22] The (*E*)-configuration of the double bond was confirmed by the large ^{1}HNMR coupling

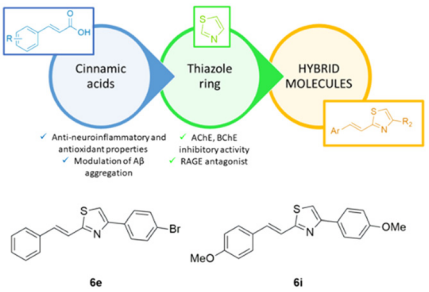

Fig. 1 Design of styryl-thiazole hybrids.

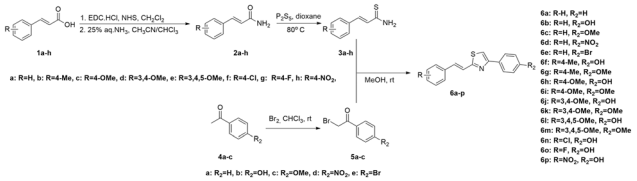

Scheme 1 Synthesis of styryl-thiazole hybrids **6a–p**.

constant (~16 Hz). Additionally, the conversion of the amide to the corresponding thioamide was confirmed by the significant downfield shift (~30 ppm) of the thiocarbonyl signal in ^{13}CNMR to ~200 ppm.

Compounds **5a–c** were prepared from the corresponding acetophenones **4a–c**[23,24] while **5d–e** were commercially available. Using the Hantzsch thiazole synthesis,[25,26] α-bromo carbonyl compounds **5a–e** were reacted with thioamides **3a–h** to provide *E*-styryl thiazole hybrids **6a–p** in medium to good yields (25–88%) after purification.

Biological studies

Human neuroblastoma SH-SY5Y cells provide a useful model for *in vitro* research, especially for neurodegenerative disorders such as Parkinson's and Alzheimer's diseases.[27] To investigate the anti-AD potential of **6a–p**, SHSY-5Y cells, treated with retinoic acid (RA)/brain-derived neurotrophic factor (BDNF), were differentiated into mature neuron-like cell cultures to obtain an AD *in vitro* experimental model.[28] First, cytotoxicity studies on SHSY-5Y cells were performed for all the synthesized compounds **6a–p** in the range of concentrations between 12.5 and 100 μg mL^{-1} (Fig. 2). Results showed that only **6e** and **6i** were found to have biocompatible properties showing no cytotoxic effect on the differentiated SHSY-5Y cells (Fig. 2) compared to the other compounds.

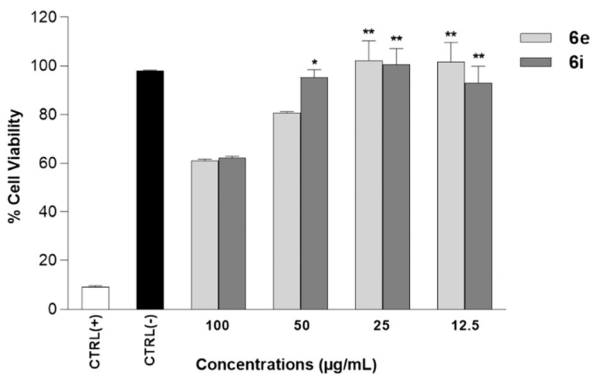

Fig. 2 Cell viability assays of **6e** and **6i** on the human neuroblastoma RA/BDNF differentiated SH-SY-5Y cells. SH-SY-5Y cells were incubated for 24 h with **6e** and **6i** (12.5–100 μg mL^{-1}) and then the % cell viability was assayed by MTT test. (–) Ctrl: untreated cells. (+) Ctrl: cells treated with 1.0% Triton X-100. Data are presented as the means ± SD for three independent experiments (n = 3). *p < 0.05 and **p < 0.01 significative *vs.* (+) Ctrl.

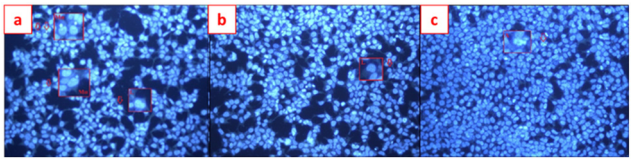

Fig. 3 Hoechst 33258 fluorescent staining analysis for genotoxicity assessments. a) Negative control – 20× magnification, b) compound **6e** – 20× magnification, and c) compound **6i** – 20× magnification. MN, micronucleus; L, lobbed nuclei, N, notched nuclei, and A, apoptotic.

Starting from these data, the genotoxic properties of **6e** and **6i** were also assessed on the differentiated SHSY-5Y cells. Genotoxic analysis of **6e** and **6i** by using Hoechst 33258 fluorescent nuclear staining showed that both **6e** and **6i**, tested at the concentration of 100 μg mL^{-1}, did not enhance the genotoxic properties on the differentiated SHSY-5Y cells. In fact, in the negative control, 16 abnormal nuclear structures were observed (0.016 NA/1000 cells ± SD), comparable to the cells treated with **6e** and **6i** (0.017 NA/1000 cells ± SD) (Fig. 3 and Table 1).

The present investigation aimed to study the neuroprotective potential of **6e** and **6i** from degeneration associated with the $A\beta_{1-42}$ in human neuroblastoma SH-SY5Y cells, chosen as an experimental *in vitro* AD model.

The AD *in vitro* cell model was generated by treating the SH-SY5Y cells with $A\beta_{1-42}$ at the concentration of 20 μM for 24 h (data not shown). Results revealed that **6e** and **6i** were able to significantly increase cell viabilities compared to $A\beta_{1-42}$-exposed cell cultures. **6i** at the concentration of 50 μg mL^{-1} and **6e** at the concentration of 25 μg mL^{-1} resulted in ~34% and ~30% increase in cell viabilities, respectively (Fig. 4).

Moreover, the neuroprotective mechanisms of **6e** and **6i** were investigated by using acetylcholinesterase (AChE), beta secretase (BACE) activity assays, and $A\beta_{1-42}$ aggregation analyses. AChE activity results showed that experimental AD model cell cultures have higher AChE activity (459.6 ± 32.152 mU mL^{-1}, 20 μM of $A\beta_{1-42}$ exposure) compared to differentiated SHSY-5Y cell culture (363.6 ± 32.152 mU mL^{-1}, negative control). Compounds **6e** and **6i** exhibited high AChE inhibitory properties in the experimental AD model at 375.6 ± 18.425 mU mL^{-1} and 397.6 ± 32.152 mU mL^{-1}, respectively (Table 2). Furthermore, the BACE activity assay showed that $A\beta_{1-42}$ application to the differentiated SHSY-5Y cell culture significantly increased BACE activity from 10.31 ± 0.82 (β-secretase activity, relative fluorescence units per mg protein) to 54.35 ± 4.34. On the other hand, **6e** (17.41 ± 1.39) and compound **6i** (14.13 ± 1.13) applications significantly ameliorated the negative impact of $A\beta_{1-42}$ exposure on the BACE enzyme activity (Table 3).

Both synthesized derivatives **6e** and **6i** were also tested to evaluate their intrinsic ability to inhibit both AChE and BACE1 enzymes (Fig. 5). The eserine, or physostigmine, is a well-characterized inhibitor of AChE – an enzyme responsible for the hydrolysis of the neurotransmitter acetylcholine in synaptic clefts – and was used as a recognized standard. Among the tested compounds, **6i** showed the best ability to inhibit AChE with IC_{50} of 63.6 μg mL^{-1}, while the weakest inhibitory activity was found in the case of **6e** (IC_{50} = 78.5 μg mL^{-1}). These data also confirmed a correlation between the increase in concentration and the percentage of inhibition for both derivatives.

We used OM99-2 – a well-recognized inhibitor of the BACE1 enzyme – as a positive control to validate the assay conditions, ensuring that they are conducive to BACE1 inhibition. The IC_{50} of **6e** and **6i** against BACE1 was 15.2 μg mL^{-1} and 25.3 μg mL^{-1}, respectively (Fig. 6). The results indicated that the most active compound was **6e**. Also, in this case, there was a dose-dependent effect: the percentage of inhibition increased with the enhancement of the concentration of compounds.

Moreover, the impact of **6e** and **6i** on the $A\beta_{1-42}$ aggregations was investigated by using the Congo red staining technique. Analyses showed that **6e** and **6i** have a positive impact on $A\beta_{1-42}$ aggregation in the experimental AD model. According to the results, **6i** has the highest potential against $A\beta_{1-42}$ aggregation with over 80% preventive activity (Fig. 7).

Flow cytometry analyses put forth that the $A\beta_{1-42}$-induced cell death mechanism produced 36% apoptosis and 9% necrosis in the differentiated SHSY-5Y cell cultures (Fig. 8B). Hybrid **6i** at the concentration of 50 μg mL^{-1} reduced the apoptotic cell death ratio by 30% and decreased necrotic cell deaths by 6% (Fig. 8C). On the contrary, **6e** at lower concentrations (25 μg mL^{-1}) resulted in the most effective treatment against $A\beta_{1-42}$-induced apoptosis by reducing apoptosis by 20% and necrosis by 5%.

Docking studies

To support the experimental results obtained by enzymatic inhibition, the interaction between AChE, BACE, and tested

Table 1 Nuclear abnormalities (NA) of SHSY-5Y cells treated with compounds **6e** and **6i** were obtained from Hoechst 33258 fluorescent staining analysis

Treatment	Total MN	Total lobbed	Total notched	Mean NA/1000 cells ± SD
(−) Ctrl	6	5	5	0.016 ± 0.007[a]
6e	4	5	9	0.017 ± 0.007[a]
6i	6	6	5	0.017 ± 0.008[a]

(−) Ctrl: cell culture plate. MN: micronucleus. Data are presented as the means ± SD for three independent experiments (n = 3). [a] $p < 0.05$ significative *vs.* (−) Ctrl.

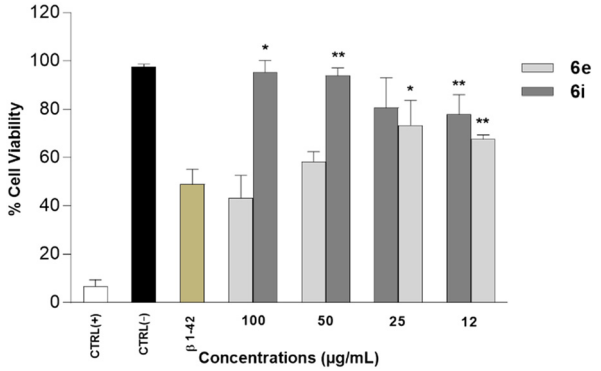

Fig. 4 Neuroprotective properties of **6e** and **6i** (12.5–100 μg mL^{-1}) against $A\beta_{1-42}$-treated SH-SY-5Y cells assayed by MTT assay (−) Ctrl: untreated cells. (+) Ctrl: cells treated with 1.0% Triton X-100. Data are presented as the means ± SD for three independent experiments (n = 3). *$p < 0.05$ and **$p < 0.01$ significative *vs.* (+) Ctrl.

Table 2 Acetylcholinesterase (AChE) activity in the experimental AD model with respect to **6e** and **6i** applications for 24 h

Compound	AChE activity (mU mL^{-1})
(−) Ctrl	363.6 ± 32.152[a]
(+) Ctrl	459.6 ± 32.152[b]
6e	375.6 ± 18.425[a]
6i	397.6 ± 32.152[a]

One milliunit (mU) of AChE activity was defined as the number of nmoles of acetylcholine hydrolyzed per min at 22 °C. (−) Ctrl: non-treated differentiated SH-SY5Y cells; (+) Ctrl: $A\beta_{1-42}$-treated cells. Different letters (a, b) in the same column present statistical differences from each other.

compounds **6e** and **6i**, molecular docking studies were performed.

Fig. 7–10 show the protein–ligand interaction of the synthesized hybrids **6e** and **6i** with the human AChE (Fig. 9 and 10) and BACE enzymes (Fig. 11 and 12). It can be observed from investigations that the highest binding energy is −5.20 kcal mol^{-1} and the lowest binding energy is −9.58 kcal mol^{-1} between the different compounds and AChE enzyme. The docking analyses revealed that the binding energies between the different compounds considered in this study with the BACE are between −4.41 kcal mol^{-1} and −8.55 kcal mol^{-1}. Moreover, molecular docking analyses showed that the lowest binding energy for AChE was found at −9.58 kcal mol^{-1} which was the interaction between compound **6e** and the enzyme. The inhibition constant of compound **6e** was investigated as 95.61 nM which was the lowest one among all the other compounds. The molecular interaction distance between **6e** and AChE residue was calculated as 2.09 Å which was the closest interaction distance compared to other compounds (Fig. 7). Compound **6i** also showed high interaction capabilities with 8.52 kcal mol^{-1} binding energies to the AChE enzyme (Fig. 9). When these results were compared to *in vitro* AChE activity assays, it was observed that compound **6e** has the highest AChE enzyme inhibitory capacity and **6i** has significant inhibitory potential (Table 2). All data, both theoretical and experimental AChE inhibition investigations, were correlated with each other.

Docking analysis on the BACE enzyme showed that the lowest binding energy belongs to compound **6e** with −8.55 kcal mol^{-1}. The inhibition constant of compound **6e** was calculated as 544.52 nM and the closest interaction distance was found to be 2.27 Å (Fig. 11). According to the investigations, another strong interaction for the BACE enzyme was compound **6i** with binding energies of −8.17 (Fig. 12). Furthermore, *in vitro*, BACE activity analysis showed that compounds **6e** and **6i** exhibited strong inhibitory potential against the BACE enzyme.

Table 3 β-Secretase activity comparisons with respect to the **6e** and **6i** application to the experimental AD model for 24 h

Compound	β-Secretase activity (relative fluorescence units per mg protein)
(−) Ctrl	10.31 ± 0.82[a]
(+) Ctrl	54.35 ± 4.34[b]
6e	17.41 ± 1.39[c]
6i	14.13 ± 1.13[c]

(−) Ctrl: non-treated differentiated SH-SY5Y cells; (+) Ctrl: $A\beta_{1-42}$-treated cells. Different letters (a, b, c) in the same column present statistical differences from each other.

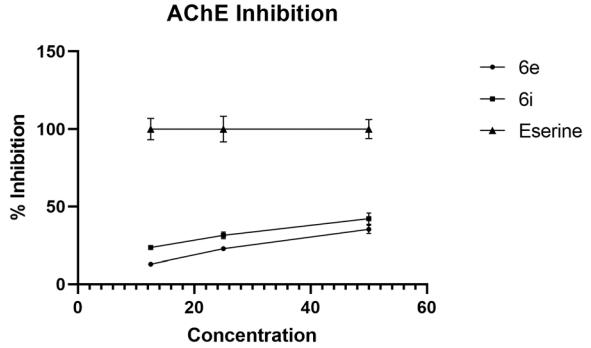

Fig. 5 *In vitro* AChE inhibitory activity of **6e** and **6i**.

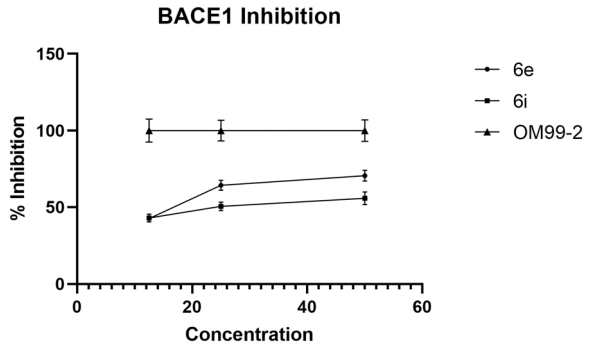

Fig. 6 BACE1 inhibitory activity of **6e** and **6i** assessed by BACE1-FRET assay.

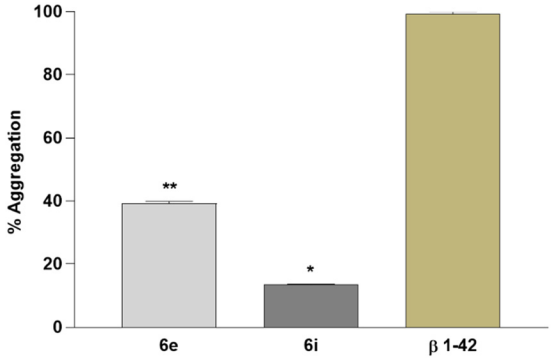

Fig. 7 *In vitro* $A\beta_{1-42}$ aggregation analysis in the experimental AD model. Data are presented as the means ± SD for three independent experiments (n = 3). *$p < 0.05$ and **$p < 0.01$.

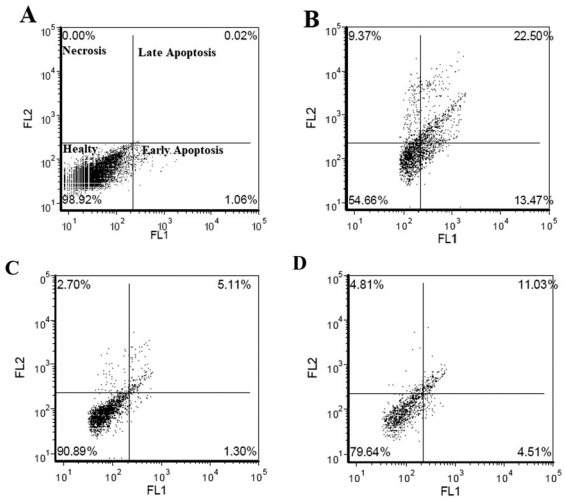

Fig. 8 Flow cytometry analysis of **6e** and **6i** on the experimental AD model for 24 h. A) Negative control; B) $A\beta_{1-42}$ treatment; C) compound **6i** (50 μg mL^{-1}); D) compound **6e** (25 μg mL^{-1}).

In silico evaluation of physicochemical properties

Inadequate efficacy and safety of a novel drug may be associated with its poor absorption, distribution, metabolism, and excretion (ADME).[29] Properties such as molecular weight (MW), hydrogen bond receptor (HBA), hydrogen bond donor (HBD), number of rotatable bonds, lipid water partition coefficient ($\log P_{O/W}$), and topological polar surface area (TPSA) can be predicted by using SwissADME program (**https://www.swissadme.ch/**). The analysis of the data obtained by this method showed that (Tables 4 and 5).

According to Table 4, only **6e** violates Lipinski's rule due to a $\log P$ value slightly higher than 5, while **6i** respects all parameters of the rule of five.

To confirm this prediction, water solubility and $\log P$ were also calculated experimentally using HPLC methods. Both hybrids **6e** and **6i** resulted from poor water solubility showing values equal to 1.75×10^{-5} and 7.19×10^{-5}, respectively.

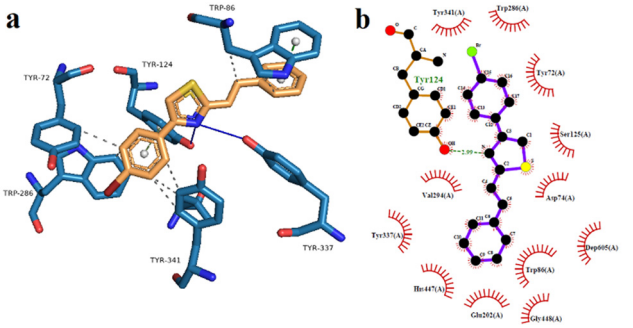

c

Protein	Compound	Distance H-A (Å)	Binding energy (Kcal/Mol)	Inhibition constant (Ki, nM)	No of H bonds (drug-enzyme)	Amino acid involved in the interaction
AChE	**6e**	2.09	- 9.58	95.61	2	Tyr (341), Tyr (337), Tur (124), Tyr (72), Trp (86), Trp (286)

Fig. 9 Binding mode of the best docking conformation of the binding mode of human AChE with **6e** obtained by a) PyMol, b) LigPlot, and c) the table of hydrogen-bonds (H-bonds) (with distance Å), binding energy (kcal mol^{-1}), inhibition constant, number of H-bonds (drug–enzyme) and amino acid involved in interaction obtained from Protein–Ligand Interaction Profiler. The blue line and dashed green show the H-bonds in PyMol and LigPlot, respectively.

The logarithm of the ratio of the concentrations of the unionized hybrids in the solvents ($\log P$) was calculated by the shake-flask method. Results confirmed the good lipophilicity of **6e** ($\log P$ = 4.87) and **6i** ($\log P$ = 4.18).

In silico pre-ADMET profile of both hybrids was predicted by using pre-ADMET software. As shown in Table 5, blood–brain barrier values (BBB) of **6e** and **6i** were in the range between 0.2 and 0.1 suggesting that both hybrids are scarcely permeable. Human gastrointestinal tract values (HIA) of these candidates are close to 98%, indicating these compounds can be well absorbed after oral administration.

Using Pre-ADMET software, both compounds showed good absorption properties (% human intestinal absorption, % HIA).[30] However, *in vitro* MDCK cell permeability values are low, revealing that both compounds are poorly permeable for oral drug absorption.[31] These values are in contrast with *in vitro* Caco-2 cell permeability values that suggested they are moderate parameters revealing that **6e**, possessing Br substituent in the *para* position of the thiazole ring, showed a slightly higher BBB penetration rate (0.20) than **6i** (0.13). Taking together all these data, **6e** could be a slightly better candidate to cross BBB than **6i** because the presence of Br in the *para* position could improve the BBB penetration rate of permeable compounds. Both compounds are strongly bound to plasma protein and are poorly soluble in water.

However, **6i** was able to inhibit the AChE and to reduce at the same time the Aβ-aggregation more effectively than **6e**. An important role was played by the nature and positions of

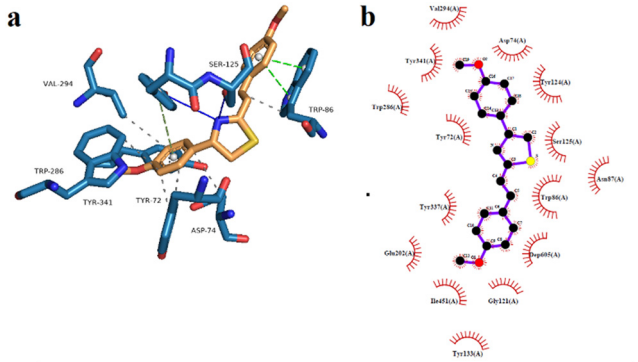

c

Protein	Compound	Distance H-A (Å)	Binding energy (Kcal/Mol)	Inhibition constant (Ki, nM)	No of H bonds (drug-enzyme)	Amino acid involved in the interaction
AChE	**6i**	1.90	- 8.52	576.88	3	Tyr (341), Tyr (72), Trp (86), Trp (286), Val (294), Ser (125), Asp (74)

Fig. 10 Binding mode of the best docking conformation of the binding mode of human AChE with **6i** obtained by a) PyMol, b) LigPlot, and c) the table of hydrogen-bonds (H-bonds) (with distance Å), binding energy (kcal mol^{-1}), inhibition constant, number of H-bonds (drug–enzyme) and amino acid involved in interaction obtained from Protein–Ligand Interaction Profiler. The blue line and dashed green show the H-bonds in Pymol and LigPlot, respectively.

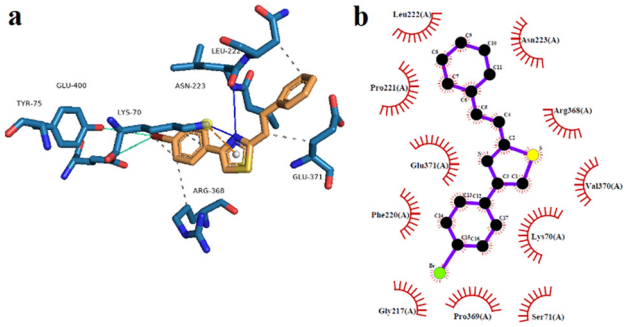

c

Protein	Compound	Distance H-A (Å)	Binding energy (Kcal/Mol)	Inhibition constant (Ki, nM)	No of H bonds (drug-enzyme)	Amino acid involved in the interaction
BACE	**6e**	2.27	- 8.55	544.52	2	Glu (400), Glu (371), Tyr (75), Lys (70), Asn (223), Leu (222), Arg (368)

Fig. 11 Interaction mode of the best docking conformation of the binding mode of human BACE with **6e** obtained by a) PyMol, b) LigPlot, and c) the table of hydrogen-bonds (H-bonds) (with distance Å), binding energy (kcal mol^{-1}), inhibition constant, number of H-bonds (drug–enzyme) and amino acid involved in interaction obtained from Protein–Ligand Interaction Profiler. The blue line and dashed green show the H-bonds in Pymol and LigPlot, respectively.

substituents on both aromatic rings of hybrid molecules. The hybrid **6i** bearing two methoxy groups at both aromatic rings emerged as the most effective inhibitor of AChE compared to **6e**. On the other hand, **6e** which had a Br in position 2 of the thiazole ring was found to be more effective than **6i** in the inhibition of BACE. The docking results showed that both hybrids were in the active sites of both enzymes in the proper orientation. As suggested by previous papers, the thiazole group forms important interactions with the amino acid present at the active site of these enzymes. Moreover, **6i** has been shown to have therapeutic potential by inhibiting the formation of Aβ aggregates. It could work by binding to Aβ and preventing its aggregation, as well as by stimulating the immune system to clear the aggregated protein.

Despite the effective pharmacological profile of **6i**, physicochemical properties are not satisfactory. Its poor water solubility and scarce ability to cross the BBB, as evidenced by *in silico* predictive models, could hinder the efficacy on *in vivo* models. So, the development of new candidates that may be effective in AD can be followed rationally.

Experimental

General

All reagents used were purchased from commercial suppliers (Aldrich, Acros, TCI). Reactions were monitored by thin-layer chromatography (TLC) carried out on 0.25 mm silica gel plates (silica gel 60F254) and components were envisioned by UV light absorbance. Purification of compounds by column chromatography was carried out on silica gel (70–230 mesh).

^{1}H and ^{13}C spectra were recorded on Bruker Avance 400 spectrometer and Varian Mercury 200 MHz. ESI mass spectral analyses were performed on a mass spectrometer, using direct sample injection. Negative or positive ion ESI spectra were acquired by adjusting the needle and cone voltages accordingly. Microanalysis (C, H, N) was performed on a Carlo Erba instrument model E1110. Analyses indicated by the symbols of the elements were within ±0.4% of the theoretical values.

The purity of **6a–p** was determined by chromatographic analyses. They were performed using an Agilent 1260 Infinity II HPLC (Agilent, Santa Clara, CA, USA) equipped with a 1260 Infinity II Quaternary Pump (model G7111A), 1260 Infinity II auto-sampler (model G7129A), a 1260 Infinity II Multicolumn Thermostat (model G7116A), and a 1260 Infinity II Diode Array Detector (model G7115A). Results were collected and integrated using Agilent OpenLAB CDS LC ChemStation software. The selected column was a Poroshell 120 EC-C18 (150 × 4.6 mm i.d., particle size 4 μm; Agilent, Santa Clara, USA), working at 20 °C. Samples were dissolved in acetonitrile (ACN) and analyzed using a mobile phase mixture of water (channel A) and acetonitrile (channel B),

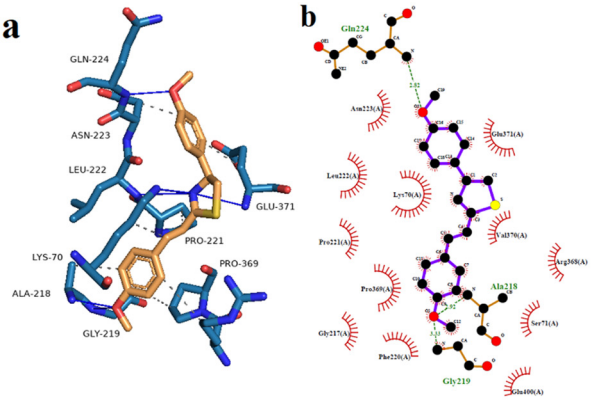

c

Protein	Compound	Distance H-A (Å)	Binding energy (Kcal/Mol)	Inhibition constant (Ki, nM)	No of H bonds (drug-enzyme)	Amino acid involved in the interaction
BACE	**6i**	1.91	- 8.17	1.03	6	Glu (371), Pro (221), Pro (369), Gly (219), Ala (218), Lys (70), Leu (222), Asn (223), Gln (224)

Fig. 12 Interaction mode of the best docking conformation of the binding mode of human BACE with **6i** obtained by a) PyMol, b) LigPlot, and c) the table of hydrogen-bonds (H-bonds) (with distance Å), binding energy (kcal mol^{-1}), inhibition constant, number of H-bonds (drug–enzyme) and amino acid involved in interaction obtained from Protein–Ligand Interaction Profiler. The blue line and dashed green show the H-bonds in Pymol and LigPlot, respectively.

both containing 0.1% v/v of trifluoroacetic acid (TFA). The flow rate was 0.8 mL min^{-1} for a total run of 15 min. The UV detector was set at a length of 254 nm.

General method for the synthesis of styryl-thiazole hybrids 6a–p

To a stirred solution of thioamide **3a–h** (1.0 mmol) in dry MeOH (7 mL) at room temperature, the corresponding phenacyl bromide **5a–e** (1.0 mmol) was added, and the reaction mixture was stirred for 1 h. Then, the volatiles were removed *in vacuo*, ethyl acetate was added, and the organic phase was washed with 5% $NaHCO_3$ and H_2O, dried over Na_2SO_4, and concentrated under reduced pressure. The crude product was purified by column chromatography using an appropriate solvent system.

(*E*)-4-Phenyl-2-styrylthiazole, 6a. Following the general method, starting from **3a** (1.80 g, 10.0 mmol) and **5a** (0.06 g, 0.30 mmol), **6a** was obtained as a yellowish solid (0.06 g) in 80% yield. R_f = 0.60 (AcOEt/PE (40–60 °C) 1 : 9). ^{1}H NMR (400 MHz, $CDCl_3$): δ 7.99 (d, J = 7.6 Hz, 2H), 7.57 (d, J = 7.3 Hz, 2H), 7.51–7.31 (m, 9H). ^{13}C NMR (101 MHz, $CDCl_3$) δ 167.0, 156.3, 135.9, 134.7, 134.5, 129.1, 129.0, 128.9, 128.4, 127.3, 126.6, 121.8, 112.3. MS (ESI) m/z calculated for $C_{17}H_{14}NS^+$ $[M + H]^+$ 264.1, found 264.2. Calcd for $C_{17}H_{13}NS$: C, 77.53; H, 4.98; N, 5.32; S, 12.18. Found: C, 77.50; H, 5.00; N, 5.34; S, 12.17.

(*E*)-4-(2-Styrylthiazol-4-yl)phenol, 6b. Following the general method, starting from **3a** (0.22 g, 1.30 mmol) and **5b** (0.28 g, 1.30 mmol), **6b** was obtained as a yellowish solid (0.10 g) in 81% yield. R_f = 0.75 (AcOEt/PE (40–60 °C) 4 : 6). ^{1}H NMR (200

Table 5 *In silico* pre-ADMET profiling of **6e** and **6i**

	6e	6i
In vivo blood–brain barrier (BBB) penetration[a]	0.2	0.13
In vitro Caco-2 cell permeability (nm s^{-1})[b]	57.80	57.08
Human intestinal absorption (HIA, %)[c]	98.21	97.42
In vitro MDCK cell permeability (nm s^{-1})[d]	0.13	0.27
In vitro plasma protein binding (%)[e]	100	94.3
Pure water solubility (mg L^{-1})[f]	0.30	0.43

[a] High absorption to CNS BBB penetration rate >2.0; middle absorption to CNS: BBB penetration rate <2.0–0.1; low absorption to CNS < 0.1. [b] Caco-2 permeability value <4: poorly permeable compound; Caco-2 permeability in the range 4–70 moderately permeable compound; Caco-2 permeability value >70: extremely permeable compound. [c] % HIA in the range 0–20: poor absorbance; % HIA in the range 20–70: moderate absorbance; % HIA in the range 70–100: good absorbance. [d] *In vitro* MDCK permeability value <25: poorly permeable compound; *in vitro* MDCK permeability value in the range 25–500: moderately permeable compound; *in vitro* MDCK permeability value >500: extremely permeable compound. [e] *In vitro* plasma protein binding value >90%: compound strongly bound; *in vitro* plasma protein binding value <90%: compound weakly bound. [f] Water solubility value <20 mg L^{-1}: low; water solubility values in the range 10–1000 mg L^{-1}: moderate; water solubility value >1000 mg L^{-1}: high.

Table 4 Prediction of physicochemical and pharmacokinetic properties of **6e** and **6i**

Hybrid	Water solubility[a] (mg mL^{-1})	Lipinski's rule				Lipinski violations[a]	TPSA[a]	MR[a]	RB[a]
		MW (g mol^{-1})	log P^a	H-bond acceptors[a]	H-bond donors[a]				
6e	1.99×10^{-5}	342.25	5.05	1	0	1	41.13	90.62	3
6i	7.24×10^{-5}	323.41	4.38	3	0	0	59.59	95.90	5

[a] Prediction SwissADME platforms water solubility, Lipinski's rule parameters, topological polar surface area (TPSA), molar refractivity (MR), and rotatable bonds (RB) were predicted using the SwissADME software. Lipinski's rule of five determines the physicochemical properties of compounds as water/octanol partition coefficient (log P), molecular weight (MW), hydrogen bond acceptors (HBA), and hydrogen bond donors (HBD). A compound is characterized by good absorption and permeability when has a MW < 500, HBD < 5, log P value < 5, and HBA < 10.

MHz, DMSO) δ 9.66 (s, 1H), 7.88–7.79 (m, 3H), 7.76–7.69 (m, 2H), 7.53 (s, 2H), 7.47–7.34 (m, 3H), 6.84 (d, J = 8.6 Hz, 2H). ^{13}C NMR (50 MHz, DMSO) δ 165.6, 157.6, 155.4, 135.6, 133.7, 128.9, 127.6, 127.3, 125.4, 121.5, 115.5, 111.4. MS (ESI) m/z calculated for $C_{17}H_{14}NOS^+$ $[M + H]^+$ 280.1, found 279.9. Calcd for $C_{17}H_{13}NOS$: C, 73.09; H, 4.69; N, 5.01; O, 5.73; S, 11.48. Found: C, 73.11; H, 4.66; N, 5.01; O, 5.75; S, 11.47.

(*E*)-4-(4-Methoxyphenyl)-2-styrylthiazole, 6c. Following the general method, using **3a** (1.80 g, 10.00 mmol) and **5c** (0.21 g, 0.90 mmol), **6c** was obtained as a yellowish solid (0.18 g) in 75% yield. R_f = 0.52 (AcOEt/PE (40–60 °C) 1 : 9). ^{1}H NMR (400 MHz, $CDCl_3$) δ 7.88 (d, J = 8.3 Hz, 2H), 7.56 (d, J = 7.5 Hz, 2H), 7.50–7.29 (m, 6H), 6.97 (d, J = 8.3 Hz, 2H), 3.85 (s, 3H). ^{13}C NMR (101 MHz, $CDCl_3$) δ 166.7, 159.8, 156.1, 136.0, 134.5, 132.3, 129.0, 127.9, 127.4, 127.2, 121.8, 114.2, 110.6, 55.5. MS (ESI) m/z calculated for $C_{18}H_{16}NOS^+$ $[M + H]^+$ 294.1, found 294.1. Calcd for $C_{18}H_{15}NOS$: C, 73.69; H, 5.15; N, 4.77; O, 5.45; S, 10.93. Found: C, 73.71; H, 5.18; N, 4.75; O, 5.44; S, 10.91.

(*E*)-4-(4-Nitrophenyl)-2-styrylthiazole, 6d. Following the general method, using **3a** (0.14 g, 0.80 mmol) and **5d** (0.20 g, 0.80 mmol), **6d** was obtained as a yellowish solid (0.18 g) in 73% yield. R_f = 0.60 (Et_2O/PE (40–60 °C) 4 : 6). ^{1}H NMR (400 MHz, DMSO) δ 8.44 (s, 1H), 8.33 (d, J = 9.0 Hz, 2H), 8.27 (d, J = 9.0 Hz, 2H), 7.74 (d, J = 7.2 Hz, 2H), 7.59 (s, 2H), 7.43 (t, J = 7.3 Hz, 2H), 7.37 (t, J = 7.3 Hz, 1H). ^{13}C NMR (101 MHz, DMSO) δ 166.9, 152.7, 146.8, 139.9, 135.4, 134.9, 129.2, 128.9, 127.5, 127.0, 124.3, 121.1, 118.4. MS (ESI) m/z calculated for $C_{17}H_{13}N_2O_2S^+$ $[M + H]^+$ 309.1, found 309.1. Calcd for $C_{17}H_{12}N_2O_2S$: C, 66.22; H, 3.92; N, 9.08; O, 10.38; S, 10.40. Found: C, 66.23; H, 3.94; N, 9.10; O, 10.35; S, 10.38.

(*E*)-4-(4-Bromophenyl)-2-styrylthiazole, 6e. Following the general method, using **3a** (0.15 g, 0.90 mmol) and **5e** (0.25 g, 0.90 mmol), **6e** was obtained as a yellowish solid (0.22 g) in 70% yield. R_f = 0.75 (AcOEt/PE (40–60 °C) 1 : 9). ^{1}H NMR (400 MHz, DMSO) δ 8.15 (s, 1H), 7.96 (d, J = 7.6 Hz, 2H), 7.73 (d, J = 7.5 Hz, 2H), 7.66 (d, J = 7.6 Hz, 2H), 7.56 (s, 2H), 7.42 (t, J = 7.3 Hz, 2H), 7.39–7.32 (m, 1H). ^{13}C NMR (101 MHz, DMSO) δ 166.3, 153.8, 135.5, 134.3, 133.2, 131.8, 129.0, 128.9, 128.1, 127.4, 121.3, 121.2, 115.0. MS (ESI) m/z calculated for $C_{17}H_{13}BrNS^+$ $[M + H]^+$ 342.0, found 342.0. Calcd for $C_{17}H_{12}BrNS$: C, 59.66; H, 3.53; Br, 23.35; N, 4.09; S, 9.37. Found: C, 59.69; H, 3.54; Br, 23.37; N, 4.06; S, 9.34.

(*E*)-4-(2-(4-Methylstyryl)thiazol-4-yl)phenol, 6f. Following the general method, using **3b** (0.10 g, 0.53 mmol) and **5b** (0.11 g, 0.53 mmol), **6f** was obtained as a yellowish solid (0.10 g) in 62% yield. R_f = 0.60 (AcOEt/PE (40–60 °C) 3 : 7). ^{1}H NMR (400 MHz, DMSO) δ 9.64 (s, 1H), 7.82 (s, 1H), 7.80 (d, J = 2.9 Hz, 2H), 7.61 (d, J = 8.1 Hz, 2H), 7.46 (d, J = 1.2 Hz, 2H), 7.22 (d, J = 8.0 Hz, 2H), 6.83 (d, J = 8.7 Hz, 2H), 2.33 (s, 3H). ^{13}C NMR (101 MHz, DMSO) δ 165.8, 157.6, 155.3, 138.6, 133.7, 132.8, 129.5, 127.6, 127.3, 125.4, 120.5, 115.5, 111.1, 21.0. MS (ESI) m/z calculated for $C_{18}H_{14}NOS^-$ $[M–H]^-$ 292.1, found 292.3. Calcd for $C_{18}H_{15}NOS$: C, 73.69; H, 5.15; N, 4.77; O, 5.45; S, 10.93. Found: C, 73.71; H, 5.17; N, 4.75; O, 5.46; S, 10.90.

(*E*)-4-(4-Methoxyphenyl)-2-(4-methylstyryl)thiazole, 6g. Following the general method, using **3b** (0.10 g, 0.53 mmol) and **5c** (0.12 g, 0.53 mmol), **6f** was obtained as a yellowish solid (0.08 g) in 48% yield. R_f = 0.66 (AcOEt/PE (40–60 °C) 2 : 8). ^{1}H NMR (400 MHz, $CDCl_3$) δ 7.87 (d, J = 8.9 Hz, 2H), 7.46 (d, J = 6.4 Hz, 1H), 7.43 (d, J = 14.3 Hz, 2H), 7.33 (d, J = 16.2 Hz, 1H), 7.25 (s, 1H), 7.20 (d, J = 8.0 Hz, 2H), 6.97 (d, J = 8.9 Hz, 2H), 3.85 (s, 3H), 2.38 (s, 3H). ^{13}C NMR (101 MHz, $CDCl_3$) δ 167.1, 159.8, 155.9, 139.2, 134.6, 133.2, 132.4, 131.5, 129.7, 127.9, 127.2, 120.8, 114.2, 110.3, 55.5, 21.5. MS (ESI) m/z calculated for $C_{19}H_{18}NOS^+$ $[M + H]^+$ 308.1, found 308.3. Calcd for $C_{19}H_{17}NOS$: C, 74.23; H, 5.57; N, 4.56; O, 5.20; S, 10.43. Found: C, 74.26; H, 5.55; N, 4.59; O, 5.19; S, 10.40.

(*E*)-4-(2-(4-Methoxystyryl)thiazol-4-yl)phenol, 6h. Following the general method, using **3c** (0.10 g, 0.51 mmol) and **5b** (0.11 g, 0.51 mmol), **6h** was obtained as a yellowish solid (0.12 g) in 77% yield. R_f = 0.74 (AcOEt/PE (40–60 °C) 1 : 1) ^{1}H NMR (400 MHz, DMSO) δ 9.63 (s, 1H), 7.80 (d, J = 8.7 Hz, 2H), 7.76 (s, 1H), 7.67 (d, J = 8.8 Hz, 2H), 7.46 (d, J = 16.2 Hz, 1H), 7.37 (d, J = 16.2 Hz, 1H), 6.98 (d, J = 8.8 Hz, 2H), 6.83 (d, J = 8.7 Hz, 2H), 3.80 (s, 3H). ^{13}C NMR (101 MHz, DMSO) δ 166.1, 160.0, 157.5, 155.2, 133.6, 128.8, 128.2, 127.5, 125.5, 119.3, 115.5, 114.4, 110.7, 55.3. MS (ESI) m/z calculated for $C_{18}H_{16}NO_2S^+$ $[M + H]^+$ 310.1, found 310.1. Calcd for $C_{18}H_{15}NO_2S$: C, 69.88; H, 4.89; N, 4.53; O, 10.34; S, 10.36. Found: C, 69.90; H, 4.91; N, 4.50; O, 10.32; S, 10.35.

(*E*)-4-(4-Methoxyphenyl)-2-(4-methoxystyryl)thiazole, 6i. Following the general method, using **3c** (0.10 g, 0.51 mmol) and **5c** (0.12 g, 0.51 mmol), **6i** was obtained as a yellowish solid (0.11 g) in 68% yield. R_f = 0.72 (AcOEt/PE (40–60 °C) 2 : 8) ^{1}H NMR (200 MHz, DMSO) δ 7.92 (d, J = 8.7 Hz, 2H), 7.78 (d, J = 33.4 Hz, 3H), 7.65 (s, 1H), 7.43 (d, J = 6.8 Hz, 1H), 7.02 (d, J = 7.3 Hz, 2H), 6.97 (d, J = 7.4 Hz, 2H), 3.80 (s, 6H). ^{13}C NMR (50 MHz, DMSO) δ 166.3, 160.0, 159.3, 154.8, 133.8, 128.9, 128.2, 127.5, 126.9, 119.2, 114.4, 114.2, 111.5, 55.2. MS (ESI) m/z calculated for $C_{19}H_{18}NO_2S^+$ $[M + H]^+$ 324.1, found 324.1. Calcd for $C_{19}H_{17}NO_2S$: C, 70.56; H, 5.30; N, 4.33; O, 9.89; S, 9.91. Found: C, 70.55; H, 5.32; N, 4.30; O, 9.88; S, 9.94.

(*E*)-4-(2-(3,4-Dimethoxystyryl)thiazol-4-yl)phenol, 6j. Following the general method, using **3d** (0.10 g, 0.45 mmol) and **5b** (0.10 g, 0.45 mmol), **6j** was obtained as a yellowish solid (0.13 g) in 88% yield. R_f = 0.73 (AcOEt/PE (40–60 °C) 1 : 1). ^{1}H NMR (400 MHz, DMSO) δ 9.63 (s, 1H), 7.81 (d, J = 8.6 Hz, 2H), 7.76 (s, 1H), 7.44 (s, 2H), 7.37 (s, 1H), 7.22 (d, J = 8.3 Hz, 1H), 6.98 (d, J = 8.4 Hz, 1H), 6.83 (d, J = 8.7 Hz, 2H), 3.83 (s, 3H), 3.79 (s, 3H). ^{13}C NMR (101 MHz, DMSO) δ 166.1, 157.5, 155.2, 149.8, 149.1, 134.0, 128.5, 127.5, 125.5, 121.2, 119.5, 115.5, 111.7, 110.6, 109.7, 55.6, 55.6. MS (ESI) m/z calculated for $C_{19}H_{18}NO_3S^+$ $[M + H]^+$ 340.1, found 340.1. Calcd for $C_{19}H_{17}NO_3S$: C, 67.24; H, 5.05; N, 4.13; O, 14.14; S, 9.45. Found C, 67.26; H, 5.04; N, 4.15; O, 14.15; S, 9.41.

(*E*)-2-(3,4-Dimethoxystyryl)-4-(4-methoxyphenyl)thiazole, 6k. Following the general method, using **3d** (0.10 g, 0.45 mmol) and **5c** (0.10 g, 0.45 mmol), **6k** was obtained as a yellowish solid (0.12 g) in 82% yield. R_f = 0.72 (AcOEt/PE (40–60 °C) 4 : 6). ^{1}H NMR (400 MHz, DMSO) δ 7.93 (d, J = 8.8 Hz, 2H), 7.86 (s, 1H),

7.46 (s, 2H), 7.38 (s, 1H), 7.22 (d, J = 8.3 Hz, 1H), 7.02 (d, J = 8.8 Hz, 2H), 6.98 (d, J = 8.4 Hz, 1H), 3.84 (s, 3H), 3.80 (s, 3H), 3.79 (s, 3H). ^{13}C NMR (101 MHz, DMSO) δ 166.3, 159.2, 154.8, 149.8, 149.1, 134.1, 128.4, 127.4, 126.9, 121.3, 119.4, 114.2, 111.7, 111.5, 109.7, 55.6, 55.6, 55.2. MS (ESI) m/z calculated for $C_{20}H_{20}NO_3S^+$ $[M + H]^+$ 354.1, found 354.2. Calcd for: $C_{20}H_{19}NO_3S$: C, 67.97; H, 5.42; N, 3.96; O, 13.58; S, 9.07. Found: C, 67.99; H, 5.43; N, 3.94; O, 13.57; S, 9.07.

(*E*)-4-(2-(3,4,5-Trimethoxystyryl)thiazol-4-yl)phenol, 6l. Following the general method, using **3e** (0.13 g, 0.51 mmol) and **5b** (0.11 g, 0.51 mmol), **6l** was obtained as a yellowish solid (0.14 g) in 76% yield. R_f = 0.60 (AcOEt/PE (40–60 °C) 3 : 7). ^{1}H NMR (400 MHz, DMSO) δ 9.63 (s, 1H), 7.82 (s, 1H), 7.80 (d, J = 2.2 Hz, 2H), 7.55 (d, J = 16.2 Hz, 1H), 7.45 (d, J = 16.1 Hz, 1H), 7.07 (s, 2H), 6.83 (d, J = 8.6 Hz, 2H), 3.84 (s, 6H), 3.69 (s, 3H). ^{13}C NMR (101 MHz, DMSO) δ 165.8, 157.6, 155.4, 153.1, 138.3, 134.0, 131.2, 127.6, 125.4, 120.9, 115.5, 111.0, 104.8, 60.1, 59.8, 56.0. MS (ESI) m/z calculated for $C_{20}H_{20}NO_4S^+$ $[M + H]^+$ 370.1, found 370.1. Calcd for: $C_{20}H_{19}NO_4S$: C, 65.02; H, 5.18; N, 3.79; O, 17.32; S, 8.68. Found: C, 65.00; H, 5.21; N, 3.81; O, 17.31; S, 8.66.

(*E*)-4-(4-Methoxyphenyl)-2-(3,4,5-trimethoxystyryl)thiazole, 6m. Following the general method, using **3e** (0.16 g, 0.60 mmol) and **5c** (0.14 g, 0.60 mmol), **6m** was obtained as a yellowish solid (0.19 g) in 82% yield. R_f = 0.80 (AcOEt/PE (40–60 °C) 1 : 1). ^{1}H NMR (400 MHz, DMSO) δ 7.94 (s, 1H), 7.91 (d, J = 9.1 Hz, 2H), 7.55 (s, 1H), 7.47 (d, J = 16.2 Hz, 1H), 7.08 (s, 2H), 7.02 (d, J = 8.8 Hz, 2H), 3.85 (s, 6H), 3.81 (s, 3H), 3.69 (s, 3H). ^{13}C NMR (101 MHz, DMSO) δ 166.0, 159.3, 154.9, 153.1, 138.3, 134.1, 131.2, 127.4, 126.9, 120.9, 114.2, 111.9, 104.8, 60.1, 56.0, 55.2. MS (ESI) m/z calculated for $C_{20}H_{20}NO_4S^+$ $[M + H]^+$ 384.1, found 384.1. Calcd for $C_{21}H_{21}NO_4S$: C, 65.78; H, 5.52; N, 3.65; O, 16.69; S, 8.36. Found: C, 65.79; H, 5.54; N, 3.66; O, 16.67; S, 8.34.

(*E*)-4-(2-(4-Chlorostyryl)thiazol-4-yl)phenol, 6n. Following the general method, using **3f** (0.11 g, 0.55 mmol) and **5b** (0.12 g, 0.55 mmol), **6n** was obtained as a yellowish solid (0.06 g) in 37% yield. R_f = 0.74 (AcOEt/PE (40–60 °C) 3 : 7). ^{1}H NMR (400 MHz, DMSO) δ 9.65 (s, 1H), 7.84–7.81 (m, 3H), 7.75 (s, 2H), 7.54 (d, J = 6.5 Hz, 2H), 7.47 (d, J = 8.5 Hz, 2H), 6.83 (d, J = 8.7 Hz, 2H). ^{13}C NMR (101 MHz, DMSO) δ 165.3, 157.6, 155.5, 134.6, 133.2, 132.3, 129.0, 128.9, 127.6, 125.3, 122.3, 115.5, 111.6. MS (ESI) m/z calculated for $C_{17}H_{13}ClNOS^+$ $[M + H]^+$ 314.0, found 314.0. Calcd for: $C_{17}H_{12}ClNOS$: C, 65.07; H, 3.85; Cl, 11.30; N, 4.46; O, 5.10; S, 10.22. Found: C, 65.06; H, 3.88; Cl, 11.33; N, 4.45; O, 5.09; S, 10.19.

(*E*)-4-(2-(4-Fluorostyryl)thiazol-4-yl)phenol, 6o. Following the general method, using **3g** (0.14 g, 0.75 mmol) and **5b** (0.16 g, 0.75 mmol), **6o** was obtained as a yellowish solid (0.15 g) in 65% yield. R_f = 0.78 (AcOEt/PE (40–60 °C) 4 : 6). ^{1}H NMR (400 MHz, DMSO) δ 9.62 (s, 1H), 7.85–7.79 (m, 5H), 7.50 (d, J = 4.0 Hz, 2H), 7.24 (t, J = 8.9 Hz, 2H), 6.84 (d, J = 8.7 Hz, 2H). ^{13}C NMR (101 MHz, DMSO) δ 165.6, 162.4 (d, J = 246.7 Hz), 157.6, 155.4, 132.5, 132.25 (d, J = 3.0 Hz), 129.4 (d, J = 8.2 Hz), 127.6, 125.4, 121.4, 115.8 (d, J = 21.7 Hz), 115.5, 111.3. MS (ESI) m/z calculated for $C_{17}H_{13}FNOS^+$ $[M + H]^+$ 298.1, found 298.2. Calcd for: $C_{17}H_{12}FNOS$: C, 68.67; H, 4.07; F, 6.39; N, 4.71; O, 5.38; S, 10.78. Found: C, 68.69; H, 4.08; F, 6.41; N, 4.69; O, 5.37; S, 10.76.

(*E*)-4-(2-(4-Nitrostyryl)thiazol-4-yl)phenol, 6p. Following the general method, using **3h** (0.06 g, 0.28 mmol) and **5b** (0.06 g, 0.28 mmol), **6p** was obtained as reddish solid (0.06 g) in 68% yield. R_f = 0.64 (AcOEt/PE (40–60 °C) 4 : 6). ^{1}H NMR (400 MHz, DMSO) δ 9.66 (bs, 1H), 8.25 (d, J = 8.8 Hz, 2H), 8.00 (d, J = 8.9 Hz, 2H), 7.93 (s, 1H), 7.83–7.79 (m, 3H), 7.66 (d, J = 16.2 Hz, 1H), 6.85 (d, J = 8.7 Hz, 2H). ^{13}C NMR (101 MHz, DMSO) δ 164.6, 157.7, 155.9, 146.9, 142.5, 131.1, 128.2, 127.6, 125.6, 125.2, 124.1, 115.6, 112.8. MS (ESI) m/z calculated for $C_{17}H_{13}N_2O_3S^+$ $[M + H]^+$ 325.1, found 324.9. Calcd for: $C_{17}H_{12}N_2O_3S$: C, 62.95; H, 3.73; N, 8.64; O, 14.80; S, 9.89. Found C, 62.97; H, 3.72; N, 8.66; O, 14.79; S, 9.87.

Biological assays

Cellular differentiation procedure. The SH-SY5Y cell line (ATCC® CRL-2266) was grown in DMEM : F12 (1 : 1, Gibco®) with 10% fetal bovine serum (FBS, Sigma-Aldrich®) and 1% penicillin/streptomycin (Sigma-Aldrich®) at 37 °C and 5% CO_2. After the cultures reached confluence, the cells were harvested by using trypsin/EDTA (Sigma-Aldrich®) and transferred into 48 well plates. To differentiate neuroblastoma cell lines to mature neuron-like cell cultures, 10 μM retinoic acid (RA) (Sigma-Aldrich®) was added to cell cultures, and cell medium (DMEM : F12 + 3% fetal bovine serum + 1% penicillin/streptomycin) was refreshed every 2 days until 8th day. Then, 25 nM brain-derived neurotrophic factor (BDNF) (Promega®) was integrated into the cultures for another 5 days to complete cellular differentiation. Differentiated cells were determined under the inverted microscope and cell cycle analysis was performed by using flow cytometry/cell cycle analysis for further confirmation of differentiation.[32]

Biocompatibility investigation by cytotoxicity and genotoxicity assays

MTT cell viability assay. Biocompatibility of **6a–6p** was investigated by cell viability analyses. Wide spectrum concentrations of **6a–6p** (15.625–1000 μg mL^{-1}) were applied to differentiated SHSY-5Y cell cultures for 48 hours. To assess cellular viability, an MTT assay was performed by using a commercially available kit (Cayman Chem. Co.®). 10 μL (5 mg mL^{-1}) of MTT solution was added to cell cultures in a 96-well plate and incubated for 3 hours at 37 °C. After the incubation period ended, 200 μL dimethyl sulfoxide (DMSO) (Sigma-Aldrich®) was added to each well to solve formed formazan crystals to obtain a blue/purple color in each well. Color intensities were measured at 570 nm by using a microplate reader (BioTek®).[33]

Genotoxicity analysis by Hoechst 33258 fluorescent nuclear staining

Possible genotoxic properties of **6e** and **6i** were investigated by using Hoechst 33258 fluorescent nuclear staining. **6e** and

6i were applied to the differentiated SHSY-5Y cell cultures for 24 h and cell culture mediums were removed from plates and cells were washed with PBS 3 times. Then, cell cultures were fixed by using 4% paraformaldehyde at 4 °C for 30 minutes. After the fixation procedure, cell cultures were washed by using PBS 3 times, and 200 μL of Hoechst 33258 fluorescent dye (1 mM) was added to cell cultures and incubated for 5 minutes at room temperature. Nuclear abnormalities (MN: micro nucleus, L: lobbed, and N: notched mutations) were observed under a fluorescent microscope. For each compound application, a total of 1000 cells were counted for triple replicates, and nuclear abnormality rations were investigated visually.[34]

Experimental Alzheimer's disease model

In vitro Alzheimer's disease model was constituted *via* the differentiation of SHSY-5Y cell culture and the integration of $A\beta_{1-42}$ into cell cultures. 20 μM of $A\beta_{1-42}$ was incubated in a cell culture medium for 24 h to produce amyloid fibrilization. After cellular differentiation, 20 μM of fibrilized $A\beta_{1-42}$ was added to cell cultures and incubated for 24 h to reach a 50% cytotoxic effect. To investigate the neuroprotective properties of **6e** and **6i**, 20 μM of fibrilized $A\beta_{1-42}$ and **6e** and **6i** were integrated into differentiated cell cultures for 24 h incubation period. The neuroprotective effect of **6e** and **6i** was observed by using an MTT cell viability assay.[35]

Biochemical investigations

Acetylcholinesterase (AChE) activity assay. AChE activity against **6e** and **6i** applications was investigated *via* the use of a commercial kit (Abcam®, UK, Cambridge) with respect to the manufacturer's instructions. Briefly, **6e** and **6i** were applied to the experimental Alzheimer's disease model for 24 h, and cells were lysed by using the kit's lysis buffer. After that, 50 μL of acetylthiocholine reaction buffer was integrated into each sample and incubated for 30 minutes at room temperature. Color shifts were measured at 410 nm by using a microplate reader.

β-Secretase (BACE) activity assay. 5×10^6 cells were harvested and washed with cold phosphate buffer (PBS). Cells were resuspended by using 100 μL of extraction buffer. Pipetting up and down several times to homogenize cell cultures. Samples were incubated for 15 minutes on ice and then centrifuged for 5 minutes at top speed at 4 °C to remove debris. Supernatants were collected into fresh tubes and kept on ice. 50 μL of samples were added to a 96-well plate and 50 μL of 2X reaction buffer was added to each well. After that, 2 μL of the β-secretase substrate was added to each well. Samples were incubated at 37 °C for 30 minutes in the dark and fluorescent intensity was measured by a fluorescent microplate reader at Ex/Em = 335/495 nm.

β-Site amyloid precursor protein cleaving enzyme 1 (BACE1) activity assay. The inhibition of the BACE1 enzyme was assessed using a specialized FRET (Forster resonance energy transfer) kit supplied by Invitrogen. The procedure strictly adhered to the instructions outlined by the manufacturer. To prepare for the assay, BACE1, which was derived from a baculovirus expression system, was combined with a specific assay buffer composed of 50 mM sodium acetate at a pH level of 4.5. This mixture resulted in a 3X working solution with a concentration of 1 unit per mL. In parallel, the peptide substrate, labeled as Rh-EVNLDAEFK-Quencher, was also diluted with the identical assay buffer to create a 3X stock solution with a concentration of 750 nM. For the inhibitors that were to be tested against BACE1, initial stock solutions in DMSO were further diluted with the assay buffer. This produced a 3X solution of the test compounds at varying concentrations. To set up the assay, a 96-well plate was used. Into each well, 10 μL of the 3X BACE1 enzyme solution was combined with 10 μL of each inhibitor sample, ensuring thorough mixing. This was followed by adding 10 μL of the 3X substrate solution to each well, marking the commencement of the reaction. The total reaction volume in each well amounted to 30 μL. After assembly, the plate was incubated at a steady temperature of 25 °C. The duration of this incubation period was 90 minutes, and it was crucial to keep the plate in the dark to prevent interference. Following the incubation, the reaction was terminated by introducing 10 μL of 2.5 mM sodium acetate to each well. After the reaction was completed, the plate was analyzed for fluorescence. The readings were taken at an excitation wavelength of 544 nm and an emission wavelength of 590 nm using a multi-well spectrofluorometer instrument.

AChE activity assay. The reaction mix, totaling 100 μL, consisted of 60 μL of a 50 mM $Na_2H\ PO_4$ buffer at pH 7.7. A 10 μL sample of the test compound (0.5 mM per well) was introduced, followed by 10 μL of enzyme (0.005 unit per well). After mixing, an initial reading at 405 nm was taken. The mixture was then warmed for 10 minutes at 37 °C. The reaction commenced upon adding 10 μL of a 0.5 mM per well substrate (acetylthiocholine iodide) and an additional 10 μL DTNB (0.5 mM per well). Post a 15-minute incubation at 37 °C, absorbance was recorded at 405 nm on a Synergy HT, Biotek, USA 96-well plate reader. Each test was performed thrice with appropriate controls. Eserine (0.5 mM per well) served as the reference standard. Inhibition percentages were determined using the equation (inhibition% = (control − test)/control × 100), and IC_{50} values were derived from the EZ-Fit Enzyme kinetics software by Perrella Scientific Inc. (Amherst, USA).

In vitro β-amyloid aggregation analysis by using Congo red staining

After **6e** and **6i** applications to the experimental disease model, cells were fixed by using 4% paraformaldehyde in phosphate-buffered saline at 4 °C for 30 min. Cultures were washed with PBS and 100 μL of Congo red (1 μM, C.I.22120, Direct Red 28; Aldrich, Milwaukee, WI) was added to each well. Samples were incubated for 1 h in the dark and washed

with PBS 3 times. To extract Congo Red dye from beta-amyloid fibrils, 100 μL of DMSO was added to each well. Color intensities were measured by using a microplate reader at 497 nm.[36]

Flow cytometry analysis

Apoptotic and necrotic status in the experimental Alzheimer's disease model against **6e** and **6i** applications were determined by using Annexin V-FITC Apoptosis Kit (Abcam®, BioVision, UK) according to the manufacturer's instructions. Briefly, 105 cells were seeded into a 48-well plate, and compounds were applied to cultures for 24 hours. Experimental analyses were divided into six groups; 20 μM of fibrilized $A\beta_{1-42}$ applied AD model, **6i** (50 μg mL^{-1}), and **6e** (25 μg mL^{-1}) applied AD model for 24 h. Cell cultures were transferred into a fresh Eppendorf tube by using trypsin incubation for 3 minutes at 37 °C. Cells were centrifuged at 500 × *g* for 5 minutes and supernatants were discarded. Cells were resuspended in 500 μL of binding buffer and 5 μL of Annexin V-FITC/5 μL of propidium iodide was added to cell cultures. After 5 min incubation at room temperature, cells were analyzed by flow cytometry (CyFlow® Cube 6, Germany).

Molecular docking

Docking investigations were performed using Auto Dock software (**https://autodock.scripps.edu**) in accordance with the previously published protocol.[37] AChE and BACE protein structures were obtained from the Protein Data Bank (RCSB PDB, **https://www.rcsb.org/**). Structures of **6e** and **6i** in PDB (Protein database) format were constituted by using ChemDraw (Chem3D) software. Then, the Auto Dock molecular modeling software was used to acquire the protein–ligand interactions. In the process, the final docking score for each molecule was calculated by taking the average score of the protein–ligand docking scores. Subsequently, the resulting average scores were ranked from highest to lowest. The obtained docking results using Auto Dock were analyzed by the Protein–Ligand Interaction Profiler (**https://plip-tool.biotec.tu-dresden.de**) online software in order to monitor the distance between ligand and amino acid residues in detail. Finally, PyMol software (**https://pymol.org**) was utilized to obtain 3-dimensional residual interaction plots, and also the LigPlot software (Version 4.5.3, **https://www.ebi.ac.uk/thornton-srv/software/LIGPLOT**) was performed to obtain data related to interactions between protein and ligand in 2-dimensional sketches.[38,39]

HPLC-UV assays

The analytical HPLC apparatus consisted of a Waters 600 HPLC pump (Waters Corporation, Milford, MA, USA). The mobile phase was a mixture of H_2O and ACN + 0.1% TFA flushing using isocratic conditions with a flow of 1 mL min^{-1}, and a Hypersil GOLD C18 column (250 × 4.6 mm) was used. Solubility was determined as previously reported.[40] The log*P* values were determined by "shake-flask" method.[41] Approximately 5 mg of compound was dissolved in 1 mL of *n*-octanol and mixed with an equal volume of phosphate buffer solution (PBS, pH 7.4). The mixture was subjected to repeated inversions (200 times, for 5 min) and then allowed to stand for 30 min for the complete separation of the two phases. Then, each phase was analyzed by HPLC.

Conclusions

In this paper, sixteen styryl thiazole hybrids were designed, synthesized, characterized, and tested as potential anti-Alzheimer drug candidates.

Docking studies confirmed the capability of the most active hybrids **6e** and **6i** to inhibit AChE and BACE, two important enzymes involved in the pathogenesis of AD. Moreover, **6i** has been shown to have therapeutic potential by inhibiting the formation of Aβ aggregates. This hybrid could be considered a potential lead compound for the development of multi-target drugs with AChE, BACE, and Aβ-aggregation inhibitory properties. All these findings encourage medicinal chemists to improve the pharmacokinetic profile of this hybrid since its water solubility and capability to cross the BBB are very low. Further research is needed to fully understand the mechanism of action and optimize its pharmacokinetic properties for clinical use.

Author contributions

The manuscript was written through the contributions of all authors. All authors have given approval to the final version of the manuscript.

Conflicts of interest

The authors declare no conflict of interest.

Acknowledgements

This research project was supported by the Italian Ministry of Education, University and Research (University "G. d'Annunzio" of Chieti-Pescara) FAR 2020 and by NKUA-ELKE K.E.16672.

Notes and references

1 H. Zhu, V. Dronamraju, W. Xie and S. S. More, *Med. Chem. Res.*, 2021, **30**, 305–352.
2 C. Cornacchia, L. Marinelli, A. Di Rienzo, M. P. Dimmito, F. Serra, G. Di Biase, B. De Filippis, H. Turkez, A. Mardinoglu, I. Bellezza, A. Di Stefano and I. Cacciatore, *Eur. J. Med. Chem.*, 2022, **243**, 114746.
3 Y. H. Ham, K. K. Jason Chan and W. Chan, *Chem. Res. Toxicol.*, 2020, **33**, 1815–1821.
4 I. Cacciatore, H. Turkez, A. Di Rienzo, M. Ciulla, A. Mardinoglu and A. Di Stefano, *RSC Med. Chem.*, 2021, **12**, 1944–1949.
5 P. K. Mandal, S. Saharan, M. Tripathi and G. Murari, *Biol. Psychiatry*, 2015, **78**, 702–710.

6 M. Rosini, E. Simoni, M. Bartolini, A. Tarozzi, R. Matera, A. Milelli, P. Hrelia, V. Andrisano, M. L. Bolognesi and C. Melchiorre, *Eur. J. Med. Chem.*, 2011, **46**, 5435–5442.
7 T. B. Callis, T. R. Garrett, A. P. Montgomery, J. J. Danon and M. Kassiou, *J. Med. Chem.*, 2022, **65**, 13483–13504.
8 H. Wang, Z. Cai, S. Zheng, H. Ma, H. Lin and X. Zheng, *Lett. Drug Des. Discovery*, 2018, **15**, 388–397.
9 B. Sever, M. D. Altintop, H. K. Gençer, H. A. Kapkaç, O. Atli, M. Baysal and A. Özdemir, *Lett. Drug Des. Discovery*, 2018, **15**, 744–756.
10 R. Hussain, H. Ullah, F. Rahim, M. Sarfraz, M. Taha, R. Iqbal, W. Rehman, S. Khan, S. A. A. Shah, S. Hyder, M. Alhomrani, A. S. Alamri, O. Abdulaziz and M. A. Abdelaziz, *Molecules*, 2022, **27**, 6087.
11 G. Ghotbi, M. Hamzeh-Mivehroud, A. Taghvimi, S. Davaran and S. Dastmalchi, *Pharm. Sci.*, 2021, **27**, 366–377.
12 K. Luo, J. Chen, H. Li, D. Wu, Y. Du, S. Zhao and X. Fu, *Bioorg. Chem.*, 2023, **138**, 106596.
13 V. K. Nuthakki, S. Choudhary, C. N. Reddy, S. Bhatt, A. Jamwal, A. Jotshi and S. B. Bharate, *ACS Chem. Neurosci.*, 2023, **14**, 1193–1219.
14 Y. S. Lee, H. Kim, Y. H. Kim, E. J. Roh, H. Han and K. J. Shin, *Bioorg. Med. Chem. Lett.*, 2012, **22**, 7555–7561.
15 A. Y. Hemaida, G. S. Hassan, A. R. Maarouf, J. Joubert and A. A. El-Emam, *ACS Omega*, 2021, **6**, 19202–19211.
16 K. Wang, J. Shi, Y. Zhou, Y. He, J. Mi, J. Yang, S. Liu, X. Tang, W. Liu, Z. Tan and Z. Sang, *Bioorg. Chem.*, 2021, **112**, 104879.
17 N. Ruwizhi and B. A. Aderibigbe, *Int. J. Mol. Sci.*, 2020, **21**, 5712.
18 Y. Chen, Y. Ma and W. Ma, *Eur. J. Drug Metab. Pharmacokinet.*, 2009, **34**, 51–56.
19 Y. Yan, X. Xu, X. Jie, J. Cheng, R. Bai, Q. Shuai and Y. Xie, *Tetrahedron Lett.*, 2018, **59**, 2793–2796.
20 R. Maity, S. Naskar and I. Das, *J. Org. Chem.*, 2018, **83**, 2114–2124.
21 J. Petrova, S. Momchilova and N. G. Vassilev, *Phosphorus, Sulfur Silicon Relat. Elem.*, 2000, **164**, 87–94.
22 D. Orr, A. Tolfrey, J. M. Percy, J. Frieman, Z. A. Harrison, M. Campbell-Crawford and V. K. Patel, *Chem. – Eur. J.*, 2013, **19**, 9655–9662.
23 L. Huang, T. Su, W. Shan, Z. Luo, Y. Sun and F. He, *Bioorg. Med. Chem.*, 2012, **20**, 3038–3048.
24 Q. Jiang, W. Sheng and C. Guo, *Green Chem.*, 2013, **15**, 2175.
25 V. Facchinetti, M. M. Avellar, A. C. S. Nery, C. R. B. Gomes, T. R. A. Vasconcelos and M. V. N. de Souza, *Synthesis*, 2015, **48**, 437–440.
26 Y. B. Yu, H. L. Chen, L. Y. Wang, X. Z. Chen and B. Fu, *Molecules*, 2009, **14**, 4858–4865.
27 L. F. Hoffmann, A. Martins, F. Majolo, V. Contini, S. Laufer and M. I. Goettert, *Neural Regener. Res.*, 2023, **18**, 1265–1266.
28 H. Turkez, I. Cacciatore, M. E. Arslan, E. Fornasari, L. Marinelli, A. Di Stefano and A. Mardinoglu, *Biomolecules*, 2020, **10**, 737.
29 C. A. Lipinski, F. Lombardo, B. W. Dominy and P. J. Feeney, *Adv. Drug Delivery Rev.*, 2001, **23**, 3–26.
30 S. Yee, *Pharm. Res.*, 1997, **14**, 763.
31 S. Yamashita, T. Furubayashi, M. Kataoka, T. Sakane, H. Sezaki and H. Tokuda, *Eur. J. Pharm. Sci.*, 2000, **10**, 195–204.
32 H. Turkez, M. E. Arslan, A. Yilmaz, F. Doru, O. Caglar, E. Arslan, A. Tatar, A. Hacımuftuoglu and A. M. Abd El-Aty, *J. Food Biochem.*, 2021, **45**, e13990.
33 A. Pagoni, L. Marinelli, A. Di Stefano, M. Ciulla, H. Turkez, A. Mardinoglu, S. Vassiliou and I. Cacciatore, *Eur. J. Med. Chem.*, 2020, **186**, 111880.
34 R. Küçükdoğru, H. Türkez, M. E. Arslan, Ö. Ö. Tozlu, E. Sönmez, A. Mardinoğlu, I. Cacciatore and A. Di Stefano, *Metab. Brain Dis.*, 2020, **35**, 947–957.
35 L. Marinelli, E. Fornasari, A. Di Stefano, H. Turkez, M. E. Arslan, P. Eusepi, M. Ciulla and I. Cacciatore, *Neuropeptides*, 2017, **66**, 52–58.
36 X. Li, X. Zhang, R. Xing, F. Qi, J. Dong, D. Li, X. Tian, B. Yu, M. Huang, L. Zhang, X. Yuan, Y. Yang, H. Wu, L. Zang, X. Mao and R. Sui, *Int. J. Biol. Macromol.*, 2021, **192**, 491–497.
37 D. Seeliger and B. L. de Groot, *J. Comput.-Aided Mol. Des.*, 2010, **24**, 417–422.
38 R. A. Laskowski and M. B. Swindells, *J. Chem. Inf. Model.*, 2011, **51**, 2778–2786.
39 S. Yuan, H. C. S. Chan and H. Zhenquan, *WIREs Comput. Mol. Sci.*, 2017, **7**, e1298.
40 I. Cacciatore, L. Marinelli, E. Fornasari, L. S. Cerasa, P. Eusepi, H. Türkez, C. Pomilio, M. Reale, C. D'Angelo, E. Costantini and A. Di Stefano, *Int. J. Mol. Sci.*, 2016, **17**, 1035.
41 P. Sozio, L. S. Cerasa, S. Laserra, I. Cacciatore, C. Cornacchia, E. S. Di Filippo, S. Fulle, A. Fontana, A. Di Crescenzo, M. Grilli, M. Marchi and A. Di Stefano, *Eur. J. Pharm. Sci.*, 2013, **41**, 187–198.

